This is the accepted manuscript made available via CHORUS. The article has been published as:

Paired electron crystal: Order from frustration in the quarter-filled band

S. Dayal, R. T. Clay, H. Li, and S. Mazumdar

Phys. Rev. B **83**, 245106 — Published 15 June 2011

DOI: 10.1103/PhysRevB.83.245106

The Paired Electron Crystal: order from frustration in the quarter-filled band

S. Dayal,[1] R.T. Clay,[1] H. Li,[2] and S. Mazumdar[2]

[1]*Department of Physics and Astronomy and HPC*^{2} *Center for Computational Sciences, Mississippi State University, Mississippi State MS 39762*

[2]*Department of Physics, University of Arizona, Tucson, AZ 85721*

We present a study of the effects of simultaneous charge- and spin-frustration on the two-dimensional strongly correlated quarter-filled band on an anisotropic triangular lattice. Our conclusions are based on exact diagonalization studies that include electron-electron interactions as well as adiabatic electron-phonon coupling terms treated self-consistently. The broken-symmetry states that dominate in the weakly frustrated region near the rectangular lattice limit are the well known antiferromagnetic state with in-phase lattice dimerization along one direction, and the Wigner crystal state with the checkerboard charge order. For moderate to strong frustration, however, the dominant phase is a novel spin-singlet paired-electron crystal (PEC), consisting of pairs of charge-rich sites separated by pairs of charge-poor sites. The PEC, with coexisting charge-order and spin-gap in two dimension, is the quarter-filled band equivalent of the valence bond solid (VBS) that can appear in the frustrated half-filled band within antiferromagnetic spin Hamiltonians. We discuss the phase diagram as a function of on-site and intersite Coulomb interactions as well as electron-phonon coupling strength. We speculate that the spin-bonded pairs of the PEC can become mobile for even stronger frustration, giving rise to a paired-electron liquid. We discuss the implications of the PEC concept for understanding several classes of quarter-filled band materials that display unconventional superconductivity, focusing in particular on organic charge transfer solids. Our work points out the need to go beyond quantum spin liquid (QSL) concepts for highly frustrated organic charge-transfer solids such as κ-(BEDT-TTF)$_2$Cu$_2$(CN)$_3$ and EtMe$_3$Sb[Pd(dmit)$_2$]$_2$, which we believe show frustration-induced charge disproportionation at low temperatures. We discuss possible application to layered cobaltates and $\frac{1}{4}$-filled band spinels.

PACS numbers: 71.10.Fd,75.10.Kt,74.20.Mn

I. INTRODUCTION

Strong Coulomb electron-electron (e-e) interactions can drive transitions from metallic to exotic insulating states, the most well known of which are the Mott-Hubbard semiconductor (MHS) and the Wigner crystal (WC). The MHS is a characteristic of systems with carrier concentration per site $\rho = 1$ and is driven by strong onsite e-e repulsion, the Hubbard U interaction. Depending upon the lattice structure the critical U at which the metal-insulator (MI) transition occurs, U_c, can be 0^+ or finite[1–4]. In contrast, the WC occurs in systems with $\rho \neq 1$, and is characterized by charge-ordering (CO) , *i.e.*, a periodic arrangement of *single* charge carriers on the lattice. The WC is driven by strong onsite as well as inter-site Coulomb interactions[5]. Although in principle the WC is likely at any arbitrary ρ, it has been been studied most intensively for $\rho = \frac{1}{2}$ bipartite lattices, where the nearest neighbor (n.n) Coulomb repulsion can drive the MI transition[6,7]. The combined effects of e-e and electron-phonon (e-p) interactions are also of interest, usually in one dimension (1D), where the MHS can further exhibit the spin-Peierls (SP) transition. Importantly for our purpose here the above semiconducting states have been intensively studied over the past several decades, and are largely understood, although arguments regarding the magnitude of U_c for formation of the MHS state in specific lattices or the detailed mechanism of the MI transition may continue to persist. In the present work, we discuss a new correlated-electron semiconductor, the paired-electron crystal (PEC), that occurs in $\rho = \frac{1}{2}$ systems in the presence of moderate to strong geometric lattice frustration[8]. We believe that our work has direct application to 2:1 cationic or 1:2 anionic charge-transfer solids (CTS) that exhibit correlated insulator–SC transitions, and further applies to other inorganic strongly-correlated $\frac{1}{4}$-filled materials.

The combined effects of e-e interactions and geometric lattice frustration are of strong current interest[9,10]. The bulk of the work here is for $\rho = 1$, where the Hubbard model in the limit $U \rightarrow \infty$ reduces to the Heisenberg spin Hamiltonian. Interest in the consequences of lattice frustration stems from the seminal proposal by Anderson that the ground state of the Heisenberg antiferromagnet (HAF) model on a triangular lattice is a quantum spin liquid (QSL) with no spin ordering even at zero temperature[11,12]. A nonmagnetic insulating state has been found in numerical simulations of the Hubbard model on an anisotropic triangular lattice in between the insulating antiferromagnetic (AFM) and paramagnetic metallic (PM) states[2,3]. The type of wavefunction usually assumed to describe a QSL is often referred to as a resonating valence bond (RVB) state. Whether or not RVB states appear in the square lattice for ρ slightly different from 1, and the relationship of such states to superconductivity (SC) in doped strongly correlated semiconductors remains contentious. An extension of the RVB theory of dopant-induced SC in $\rho \neq 1$ is the proposal

that frustration-induced SC occurs in the anisotropic triangular lattice within the simple Hubbard model even for ρ exactly 1, where a narrow superconducting phase is straddled on both sides by broader PM and AFM insulator phases[13–23]. It has been claimed that this transition explains the SC in the CTS[13–24]. Recent numerical work by us and others, however, have determined that SC is absent within the $\rho = 1$ triangular lattice Hubbard model[25–27] and the earlier results are artifacts of mean-field approximations.

While the ground state of the HAF on the isotropic triangular lattice is now known to be the ordered 120° AFM rather than the originally proposed QSL state[28–30], other frustrated lattices, most notably the Kagomé lattice[31], have been investigated in the search for QSL states. Proposed ground states here include various types of QSL states[32–34] as well as valence-bond solid (VBS) states[35–38]. The literature on VBS states has a long history going back to the well known Ghosh-Majumdar model[39]. The common theme in works on VBS is the frustration-driven transition from the AFM state to a total spin $S = 0$ singlet state. We have found a similar frustration-driven transition from the AFM to a $S = 0$ state in strongly correlated systems with $\rho = \frac{1}{2}$, where reduction to a spin Hamiltonian is not possible.

In contrast to the voluminous literature on correlated and frustrated systems at $\rho = 1$, the literature on frustrated $\rho \neq 1$ is relatively sparse and new. The discovery of SC[40] in hydrated Na_xCoO_2 has spurred interest in correlated systems away from $\rho = 1$[41–43], although to the best of our knowledge only isotropic triangular lattices have been studied. We will specifically focus on $\rho = \frac{1}{2}$ within the present work—on the triangular lattice with varying anisotropy. In the square lattice limit at this density, we show that spontaneous in-phase dimerization occurs in the presence of electron-phonon interactions modulating n.n hopping integrals, leading to an *effective* $\rho = 1$ system with one electron per dimer and AFM order. This result is the origin of the so-called the dimer Mott-Hubbard model[44,45] that is commonly used to describe the 2:1 cationic or 1:2 anionic organic CTS. Very recently we have proposed that under the influence of lattice frustration this dimer Mott-Hubbard AFM state gives way to a spin-paired state that we termed the PEC[8]. The PEC is different from any of the above more well known correlated semiconducting states in that it is a WC of Heitler-London spin-singlets—simultaneously charged-ordered and spin $S = 0$. Alternately, the PEC is the $\rho = \frac{1}{2}$ equivalent of the $\rho = 1$ VBS. A conceptually similar state was postulated for the electron gas many years back by Moulopoulos and Ashcroft[46,47]. There is a fundamental similarity between this earlier work and ours, in that in both cases the pairing is driven by the exchange interaction. Our previous work[8] only considered a limited set of parameters, and the full phase diagram was not discussed. Here we give a more complete phase diagram, including the competition with the WC state that was ignored before. As with the VBS state at $\rho = 1$, the PEC is a consequence of frustration-induced quantum effects. Its extraordinary stability at $\rho = \frac{1}{2}$ is a commensurability effect (recall that MHS and WC formation also require commensurability).

In section II we introduce the model we consider. We include e-p interactions to stabilize the lattice dimerization that gives the effective $\rho = 1$ dimer lattice. We present the physical mechanism behind the PEC formation by briefly discussing simple molecular clusters, for which we show that spin-singlet formation in $\rho = \frac{1}{2}$ necessarily requires charge disproportionation. The charge disproportionation in the infinite one-dimensional (1D) chain and the so-called zigzag ladder leads to periodic CO, viz., the simplest PECs. Following the discussions of these simple cases, we introduce the two-dimensional (2D) lattice that will be the focus of this work, and discuss the different possible phases. In section III we present out numerical results for the 2D system, covering a wide region of parameter space. In section IV we discuss the relevance of our results for several classes of $\rho = \frac{1}{2}$ materials and the outlook for understanding unconventional SC. We particularly emphasize the cases of the organic charge-transfer solids CTS κ-(BEDT-TTF)$_2$Cu$_2$(CN)$_3$ and EtMe$_3$Sb[Pd(dmit)$_2$]$_2$ which have been described as QSLs within the effective $\rho = 1$ scenario[48–56]. We believe frustration-induced charge disproportionation is an alternate possibility.

II. THEORETICAL MODEL

A. Hamiltonian

The Hamiltonian we consider contains electron hopping, semi-classical inter-site and onsite e-p couplings, and onsite and n.n. Coulomb interactions:

$$\begin{aligned} H &= -\sum_{\nu,\langle ij\rangle_\nu} t_\nu(1+\alpha_\nu\Delta_{ij})B_{ij} + \frac{1}{2}\sum_{\nu,\langle ij\rangle_\nu} K^\nu_\alpha \Delta^2_{ij} \\ &+ \beta\sum_i v_i n_i + \frac{1}{2}K_\beta\sum_i v_i^2 \\ &+ U\sum_i n_{i\uparrow}n_{i\downarrow} + \frac{1}{2}\sum_{\langle ij\rangle} V_{ij} n_i n_j. \end{aligned} \tag{1}$$

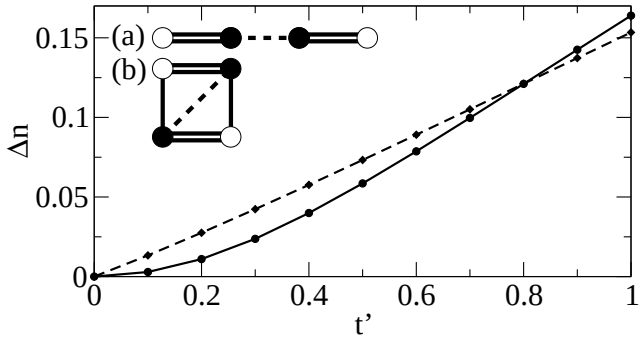

FIG. 1: Charge difference Δn between members of the same dimer as a function of the hopping integral t' corresponding to the dotted bonds, for the two molecules (a) and (b) given as inserts. Each 4-atom molecule contains two electrons. The intra-dimer double bonds have strength $t_1 = 1.5$, and the single bonds in (b) are $t_2 = 0.5$. The results shown are for $U = 4$ and $V = 0$. Solid (dashed) curves show Δn for the linear (square) molecules. Lines are guides to the eye. Filled and empty circles of the molecules correspond to sites with charge densities $0.5 + \Delta n/2$ and $0.5 - \Delta n/2$, respectively.

In Eq. 1, ν indexes the different bond directions in the lattice; for example $\nu = x$ in 1D and $\nu = \{x, y\}$ in the 2D square lattice. Our actual calculations (see below) are exact diagonalizations for a 4×4 anisotropic triangular lattice, $\nu = \{x, y, x + y\}$. $B_{ij} = \sum_\sigma (c^\dagger_{i\sigma} c_{j\sigma} + H.c.)$ is the electron hopping between sites i and j with electron creation (annihilation) operators $c^\dagger_{i\sigma}$ ($c_{i\sigma}$). α_ν is the inter-site e-p coupling constant, K^ν_α is the corresponding spring constant, and Δ_{ij} is the distortion of the bond between sites i and j. v_i is the intra-site phonon coordinate and β is the intra-site e-p coupling with corresponding spring constant K_β. Both Δ_{ij} and v_i are determined self-consistently[57]. α_ν are in general taken close to the minimum value needed for the transition to occur, our goal being the replication of the same instability from finite cluster calculations that would occur in the infinite system for 0^+ coupling. U and V_{ij} are on-site and n.n. Coulomb interactions, respectively. The physically relevant range of V_{ij} is $V_{ij} < \frac{U}{2}$ based on comparison between $\rho = 1$ and $\rho = \frac{1}{2}$ CTS[58].

B. Coupled spin-singlet and CO at $\rho = \frac{1}{2}$

We first present a simple qualitative discussion of coupled spin-singlet and CO formation at $\rho = \frac{1}{2}$. The ideas are quite general and we argue that the mechanism is *independent* of dimensionality. The key requirement is that the density must be exactly $\rho = \frac{1}{2}$, as the effect requires commensurability. Consider a single dimer of two sites with one electron. The electron populations per site are 0.5 each, but the quantum mechanical wavefunction for the system is the superposition $\frac{1}{\sqrt{2}}|10+01\rangle$, where 1 and 0 are site charge densities. If one now brings two of these dimers together, as in insert (a) of Fig. 1, the composite wavefunction of the two-dimer system can be written as $\frac{1}{2}|1010+1001+0110+0101\rangle$. If the two electrons are in a spin-singlet state then within the simple Hubbard Hamiltonian the configuration 0110, in which singlet stabilization can occur from a single n.n. hop that creates a virtual double occupancy, must dominate over the configurations 1010 and 1001, in which singlet stabilization requires two and three hops, respectively. Thus as the singlet bond between the dimers gets stronger we expect a charge difference Δn between sites belonging to the same dimer (nominally between sites 1 and 2, or between sites 3 and 4 in the linear chain of Fig. 1). While some charge disproportionation must occur in finite linear chains from end effects alone, we note that our proposed picture demands that similar charge disproportionation occurs between members of the same dimer even in the case of the periodic molecule shown in the insert (b) of Fig. 1. In this case the charges on the sites connected by the diagonal bond must be larger than 0.5, while the charges on the two other sites must be smaller. Importantly, the modulation of charge density, bond orders, as well as spin-singlet pairing all occur cooperatively, and any of these observables may be used as an order parameter in the case of a real transition. In Fig. 1 we have plotted Δn versus the hopping integral t' corresponding to the dotted bonds in the molecules shown in the insert, for the ground spin-singlet state. In both cases, as t' increased from zero Δn becomes nonzero and increases with t'. Importantly, in the spin-triplet $S = 1$ state the sign of Δn is reversed in the cyclic molecule, indicating repulsive interaction among the electrons.

Coupled CO and singlet formation occur also in the SP state in 1D $\rho = \frac{1}{2}$ systems[57–59]. A key difference from the SP transition in $\rho = 1$ is that for $\rho = \frac{1}{2}$, a MI transition first occurs at a intermediate temperature, followed by the SP transition at low temperature. For $\rho = \frac{1}{2}$, the MI leads to either a bond-dimerized or to a charge-ordered WC state with equal bond lengths[58]. Provided the n.n. Coulomb interaction is not too strong, a SP transition occurs

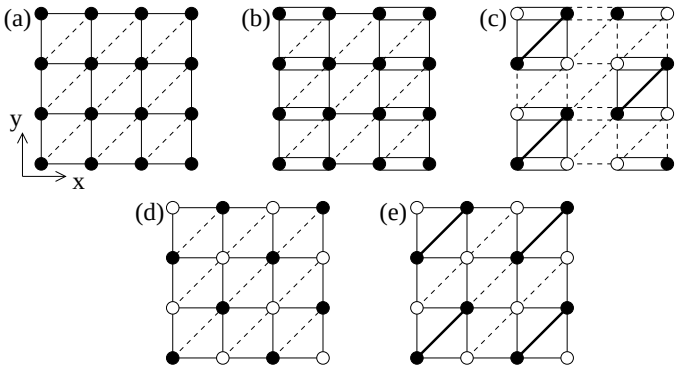

FIG. 2: (a) 2D lattice used for calculations in this paper, a square lattice with hopping $t_x = t_y \equiv t$ and frustrating bond $t_{x+y} \equiv t'$ (dashed lines). (b) Dimerized lattice. Double (single) lines indicate stronger (weaker) bonds. Site charge densities are uniform in both (a) and (b). (c) The PEC state as it occurs in this lattice. Filled (open) circles correspond to sites with charge density $\rho = 0.5 + \delta$ ($\rho = 0.5 - \delta$)[8]. Heavy line shows the location of singlet-paired sites. (d) Wigner crystal charge ordering occurring for large V_x and V_y. (e) Wigner crystal-spin gap phase with bond alternation along diagonal directions. See section III B.

from either insulating state[58], resulting in a ground state with period-4 CO $\cdots 0110 \cdots$. This state is the simplest realization of the PEC and may visualized as a second dimerization of dimer units of molecules; the singlet bond giving the spin gap (SG) forms *between* adjacent dimer units. The intermediate temperature bond-dimerized states, WC state, and PEC state with SG are all found experimentally in quasi-1D CTS[58].

Zigzag ladder systems, coupled two-stack systems in which each site on one stack is coupled to two sites on the other stack, are a second realization of the PEC state. CTS zigzag ladder materials that are $\rho = \frac{1}{2}$ have been found with spin-gap transition temperatures much larger than in 1D $\rho = \frac{1}{2}$ SP materials[60]. The insulating ground state in this case may be understood again as a PEC state occurring in a zigzag ladder lattice, with singlet bonds oriented between the two chains[61]. Unlike the 1D case, bond orders are now modulated in several lattice directions, leading to a larger SG than for the 1D PEC case[61]. Interestingly, in both the linear chain and the zigzag ladder, the $\rho = \frac{1}{2}$ PEC is obtained by simply removing alternate spin-singlet bonds from the corresponding $\rho = 1$ VBS, and replacing them with pairs of vacancies.

C. Competing broken symmetries in 2D

In this paper we will focus on ground state solutions of Eq. 1 in 2D in the presence of variable lattice frustration. The lattice we choose is a 4×4 2D square lattice with a single frustrating bond, as shown in Fig. 2(a). Thus $\nu = \{x, y, x+y\}$ within Eq. 1 for this lattice. In most of the results we will present, $t_x = t_y \equiv t$, although we will also consider $t_x \neq t_y$ in some cases. Energies will be given in units of t. We will take the frustrating bond $t_{x+y} \equiv t'$ in the range $0 \leq t' < 1$, covering the wide region between the unfrustrated square lattice ($t' = 0$) and the nearly isotropic triangular lattice ($t' = 1$). For the inter-site e-p coupling, unless denoted otherwise we choose $\alpha_x = \alpha_y \equiv \alpha$ and $\alpha' = 0$, with similarly identical spring constants $K^x_\alpha = K^y_\alpha \equiv K_\alpha$. As noted before, all bond distortions and charge densities are obtained self-consistently[57]. For all calculations we assume periodic boundary conditions.

Our calculations are largely for $V_x = V_y$, but variable $V_{x+y} \equiv V'$. In Reference 8 we presented limited numerical results for a select set of Coulomb interaction parameters ($U = 4$, $V_x = V_y = 1$, $V' = 0$) demonstrating transition from Néel antiferromagnetism to the PEC state in this lattice when t' exceeds a critical value t'_c. For completeness and for giving an introduction to the various competing states in 2D we briefly review these results here. For small t', the self-consistent solution of Eq. 1 gives spontaneous dimerization along the x axis as shown in Fig. 2(b). The dimerized lattice state is effectively $\frac{1}{2}$-filled with one carrier per dimer and has Néel AFM order between dimers for finite U. The Néel order is very clearly observable from the spin-spin correlations calculated for 4×4 clusters[8]. Importantly, the charge density $\langle n_i \rangle$ of all sites is exactly 0.5.

As t' increases, frustration reduces the strength of the antiferromagnetic correlations. Provided the n.n. Coulomb interaction V_{ij} is not too strong (see below), at a critical $t' = t'_c$ antiferromagnetic correlations disappear and charge disproportionation develops, with the charge densities within each dimer becoming inequivalent. This is shown in Fig. 2(c). In this state, the charge densities follow the pattern $\cdots 1100 \cdots$ along the x and $x + y$ directions, and the pattern $\cdots 1010 \cdots$ along the y direction. The bond distortion is period-4 along x and period-2 along y. The strongest bond orders $\langle B_{ij} \rangle$ occur between adjacent charge-rich '1–1' sites in the $x + y$ direction. Importantly, the spin-spin

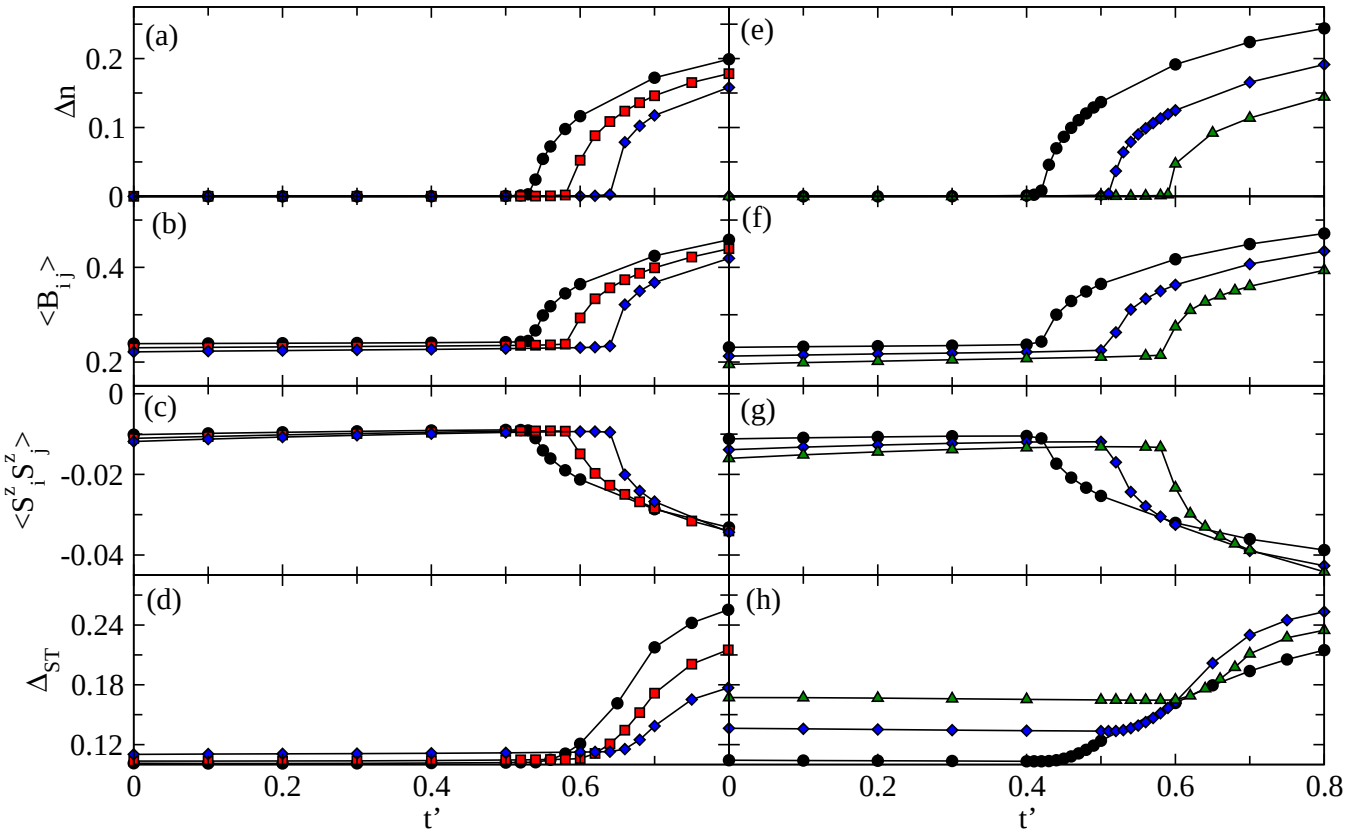

FIG. 3: (Color online) Order parameters for the 4×4 lattice versus t'. Parameters are $\alpha = 1.1$, $\beta = 0.1$, and K_α=K_β=2. Circles, squares, diamonds, and triangles are for $U = 2$, 3, 4, and 6, respectively. $V_x = V_y = V' = 0$ for (a)–(d), and $V_x = V_y = 1$ and $V' = 0$ for (e)–(h). (a) and (e) show the charge disproportionation Δn, (b) and (f) the bond order $B_{i,j}$ between charge-rich sites i and j connected by t' (see Fig. 2(c)), (c) and (g) spin-spin correlations between these sites, and (d) and (h) the singlet-triplet gap $\Delta_{\rm ST}$. In all cases the CO pattern is as shown in Fig. 2(c). For all plots lines are guides to the eye.

correlations change dramatically for $t' > t'_c$. They are strongly negative between the bonded '1–1' sites along the $x + y$ direction (see Fig. 2(c)), and are nearly zero between either member of the pair and all other sites, indicating the formation of spin-singlet bonds[8]. Any of the observables Δn, bond order between the charge-rich sites, or z-z spin correlations, $\langle S^z_i S^z_j \rangle$, may be used as order parameters for the PEC state[8].

In section III we present further details of the PEC phase and the full parameter dependence of Eq. 1, with the goal of demonstrating that *(i) the transition to the PEC that we are interested in is driven by quantum effects due to frustration only; and (ii) the PEC occurs over a broad region of parameter space.* Given the number of parameters in Eq. 1, it should be relatively easy to generate CO driven by specific (presumably artificial) choices of V_{ij}. Such classical results would be uninteresting. We therefore consider several distinct choices of Coulomb interactions: (i) $U > 0$ and all $V_{ij} = 0$, (ii) $U > 0$, $V_x = V_y = V$, and $V' = 0$, (iii) $U > 0$ and $V_x = V_y = V' = V$. PEC formation occurs in all of these parameter regions. We also show that for sufficiently strong n.n. Coulomb interactions corresponding to parameter region (ii), the WC phase with checkerboard CO (Fig. 2(d)-(e)) is the ground state of Eq. 1. We also will consider other modifications of the basic lattice, viz., sign of t' opposite site to t, and $t_x \neq t_y$. Finally, we will argue that our results are not consequences of finite size effects and are to be expected in the thermodynamic limit.

III. RESULTS

A. $U > 0$, $V_x = V_y = V' = 0$

Figs. 3(a)-(d) show the charge disproportionation Δn, bond order $\langle B_{ij} \rangle$, n.n. z-z spin-spin correlation $\langle S^z_i S^z_j \rangle$, and spin gap Δ_{ST} as a function of t'. Δ_{ST} is defined as the excitation energy from the ground $S = 0$ state to the lowest $S = 1$ state. U here is finite but all V terms are zero. Sites i and j in Figs. 3(b)-(c) correspond to two '1' sites in the

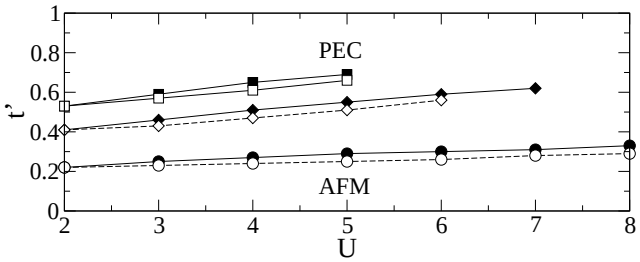

FIG. 4: Phase diagram as a function of t' and U, for $\beta = 0.1$, and $K_\alpha = K_\beta = 2$. Squares are the AFM–PEC phase boundary for $\alpha = 1.1$ and $V_x = V_y = V' = 0$; Diamonds are for $\alpha = 1.1$, $V_x = V_y = 1$, and $V' = 0$; Circles are for $\alpha = 1.2$, $V_x = V_y = 1$, and $V' = 0$. For each case, filled (open) points correspond to positive (negative) t'. Lines are guides to the eye.

PEC state connected by a t' bond (filled circles connected by heavy lines in Fig. 2(c)). As with the results in Reference 8 which included the V_x and V_y interactions, for small t' the charge density is 0.5 on all sites, and antiferromagnetic order can be seen in the spin-spin correlations (not shown here, see Fig. 3(a) in Reference 8). Nonzero t'_c in Fig. 3 is a consequence of the nature of the diagonal bonds in Fig. 2(b); the diagonal bonds inside each plaquette with two strong dimer bonds actually strengthen the AFM, and only the inter-plaquette diagonal bonds have a frustrating effect. At small t' these two effects appear to cancel, and there is only a weak effect on the AFM.

For $t' > t'_c$, Δn becomes nonzero, with the charge pattern as shown in Fig. 2(c). Similarly, the bond order between paired '1–1' sites increases abruptly, and the z-z spin-spin correlation between these sites becomes strongly negative, and nearly zero with all other lattice sites (see Reference 8), indicating formation of a singlet bond. Although Δ_{ST} is nonzero in all cases in a finite cluster, we nevertheless see a large jump in Δ_{ST} at t'_c, also indicating spin-singlet formation. The increase in bond order strength and strength of spin-spin correlation clearly follow the same pattern as Δn.

These results show that the n.n. Coulomb interaction is not essential for formation of the PEC state. Unlike the WC phase where CO is driven by the n.n. Coulomb interaction, the PEC state is a consequence of geometric lattice frustration. Increasing U moves t'_c to larger t': U tends to strengthen the AFM phase and therefore increasing U is expected to make the AFM order persist for stronger lattice frustration. The transition also becomes more discontinuous to changes in t' as U increases, suggesting it may be continuous for small U and first order for large U.

In both the 1D and in the zigzag ladder lattice, the PEC state occurs unconditionally even in the noninteracting limit ($U = V_{ij} = 0$) for any finite e-p coupling. In these two cases, the unconditional occurrence of PECs is a consequence of simple nesting. In contrast, in the isotropic $\rho = \frac{1}{2}$ 2D band considered here, the lack of nesting forbids an unconditional Peierls transition. In agreement with this, we found that for $U \lesssim 1$, the PEC phase did not occur. Instead, the self-consistent calculations converged to disordered states with no clear charge pattern. This is an indication that in the thermodynamic limit, the preferred ground state is one of uniform charge. This result is reminiscent of that in quantum spin systems: the simplest VBS transition, the SP transition, can be predicted from nesting behavior in the 1D XY model following Jordan-Wigner transformation[62]. This is, however, not true in 2D frustrated spin systems.

B. $U > 0$, $V_x = V_y > 0$, $V' = 0$

We next consider the effect of n.n. Coulomb interactions $V_x = V_y = V$, but $V' = 0$. Figs. 3(e)-(h) show the same order parameters as in Figs. 3(a)-(d) for $V = 1$. Comparing the data with and without V, the effect of moderate V is to *strengthen* the PEC state—the magnitude of all order parameters increase when $V > 0$ for a fixed value of U. For fixed U, the AFM–PEC boundary t'_c also moves to smaller t' with increasing V. Fig. 4 shows the phase diagram in the t'-U plane for both the $V = 0$ and $V > 0$ cases. Here, for each value of U, t' was varied until the AFM–PEC transition occurred, and the first t' where Δn became nonzero was taken as the AFM–PEC boundary.

One expects that when V is above a critical value V_c, the $\cdots 1100 \cdots$ PEC CO will give way to the checkerboard WC state. In 1D, this transition occurs exactly at $V_c = 2$ in the limit $U \to \infty$, and at a larger V_c for finite U[6,57]. Previous exact diagonalization for a 2D cluster[63] (without however e-p interactions or t' as considered here) found $V_c \approx 2.1$ for $U = 10$, and showed that V_c increases when $V' > 0$.

Fig. 5 shows the evolution of Δn and diagonal bond orders with V for $U = 6$. While difficult to see in Fig. 5 due to the choice of axis scales and parameters, in the PEC region Δn increases with increasing V. For the parameters of Fig. 5 (U=6, $t' = 0.8$, $\alpha = 1.1$, $\beta = 0.1$, $K_\alpha = K_\beta = 2$) the charge order pattern changes from the PEC (Fig. 2(c)) to the checkerboard WC (Fig. 2(d)-(e)) at $V \approx 1.52$. In addition, Δn increases sharply when entering the WC phase. At

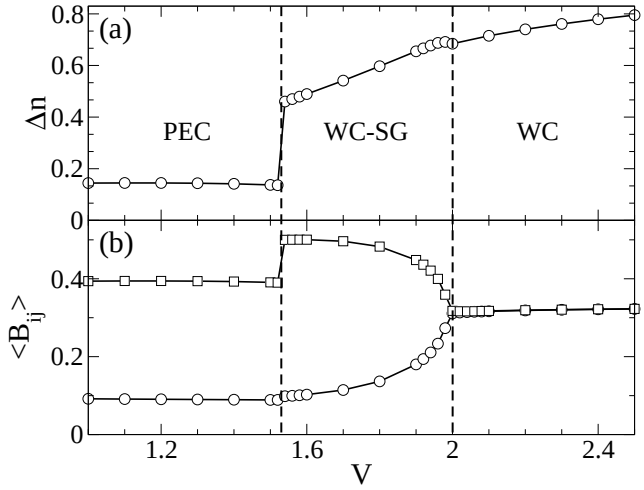

FIG. 5: Variation of order parameters with $V = V_x = V_y$ ($V' = 0$) for $U = 6$, $t' = 0.8$, $\alpha = 1.1$, $K_\alpha = K_\beta = 2$, $\beta = 0.1$. (a) charge disproportionation Δn (b) bond orders along two successive t' bonds. In PEC region, these correspond to bonds between sites with '1–1' (squares) and '1–0' (circles) occupancy. In the WC-SG and WC regions, both bonds are between '1–1' sites. Lines are guides to the eye.

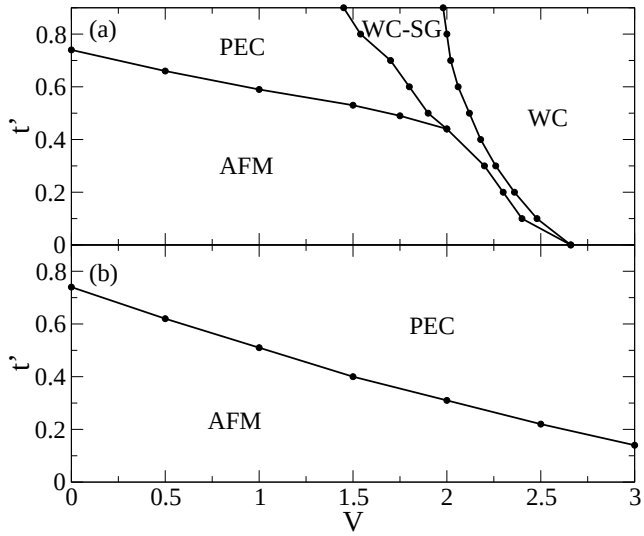

FIG. 6: (a) Phase diagram for the 4×4 lattice as a function of t' and $V = V_x = V_y$, $V' = 0$, for $U = 6$, $\alpha = 1.1$, $\beta = 0.1$, and $K_\alpha = K_\beta = 2.0$. (b) Same as (a), but with $V = V_x = V_y = V'$. For both (a) and (b), points between antiferromagnetic and PEC phases are determined as discussed in section II A; The boundary between PEC, WC-SG, and WC phases is discussed in the text. Lines are guides to the eye.

larger $V \approx 2.0$ a slight cusp occurs in the Δn versus V plot. At the same time, the pattern of bond orders changes: for $V < 2$ in the WC phase the bond orders alternate strong-weak along the $x + y$ direction (as shown in Fig. 2(e)), while for $V > 2$ the bond orders along $x + y$ are uniform (Fig. 2(d)). Within the WC phase region there are therefore two sub-phases: a phase with equal length bonds in the diagonal $x + y$ (t') directions, and a phase in which these bonds become dimerized. The added bond dimerization in the diagonal direction will result in a spin gap, and we denote this phase as the Wigner Crystal–Spin gap (WC-SG) phase. A similar spin-gapped WC phase can be found in a small region of parameter space in the 1D model[57,64].

Fig. 6(a) shows the resulting phase diagram in the t'-V plane for U=6. The V_c we find in the $t' = 0$ limit is slightly larger ($U = 6$, $V_c \approx 2.6$) than the results of Reference 63 ($U = 10$, $V_c \approx 2.1$); however, both the smaller U here as well as the e-p coupling in Eq. 1 would be expected to increase V_c. Unlike the AFM, PEC, and WC phases, the WC-SG phase is limited to a relatively narrow range of parameters. Larger lattice calculations are needed to confirm whether the WC-SG phases persists in the thermodynamic limit.

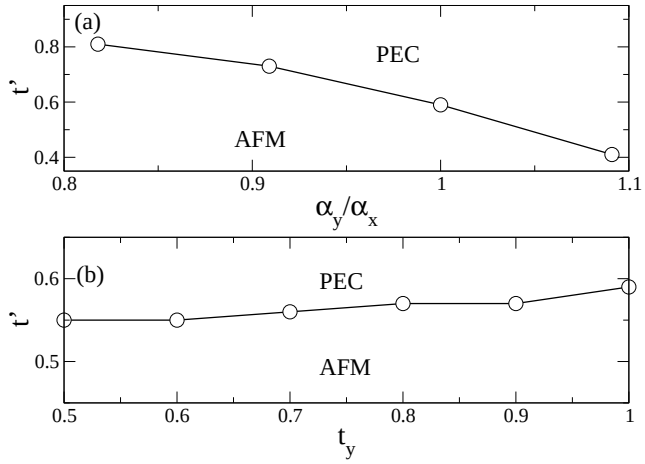

FIG. 7: Phase diagram variation on hopping and electron-phonon interaction anisotropy. In both (a) and (b), $U = 6$, $V_x = V_y = 1$, $V' = 0$, $\beta = 0.1$, and $K_\alpha = K_\beta = 2$. In (a), $t_x = t_y = 1$ and $\alpha_x = 1.1$, but α_y is varied. In (b), $t_x = 1$ and t_y is varied, with identical $\alpha_x = \alpha_y = 1.1$. Lines are guides to the eye.

C. $U > 0$, $V_x = V_y = V' > 0$

The V' interaction destabilizes the checkerboard-pattern WC, leading to a metallic phase in the absence of e-p interactions[63]. Here we will consider parameters $V_x = V_y = V' = V$. For Eq.1 without e-p interactions, $U = 10$, and $t' \leq 0.1$, exact diagonalization found[63] that in this case a metallic phase exists for V up to at least V =5. Charge fluctuations within the metallic phase adjacent to the WC were speculated to cause a CO-to-SC transition[65]. In our calculations, summarized in the phase diagram in Fig. 6(b) for $U = 6$, we also found that the WC phase does not occur, but rather than being metallic the system is insulating—either AFM at small frustration or PEC at large frustration. In this case the AFM–PEC transition can occur over a wide range of lattice frustration, $0.2 \lesssim t'_c \lesssim 0.7$. Within the PEC phase the CO pattern remains the same for all V, although Δn increases with V as in the $V' = 0$ case considered in the previous section. Although our calculations are for one value of V' only, Fig. 6(b) suggests that the PEC region is broadened relative to that in Fig. 6(a) for any $V' \neq 0$.

D. Bandstructure and electron-phonon coupling

As shown in the previous section, variation of Coulomb interactions can cause a substantial variation in the extent of frustration needed to form the PEC state. Next we show the effect of varying the one-electron parameters in Eq. 1, t_ν and α_ν.

Due to the lack of particle-hole symmetry in the anisotropic triangular lattice, differences might be expected when t' is taken as negative. However, as Fig. 4 shows, we found only a small variation in the AFM–PEC phase diagram when the sign of t' is changed. This is consistent with the expected mechanism for spin frustration in an effectively $\frac{1}{2}$-filled band: the frustrating exchange interaction is proportional to $(t')^2$, so reversing the sign of t' should only change the effective frustration at higher order.

Fig. 4 also shows the effect of changing α. As expected for a cooperative transition, stronger e-p coupling increases the size of the PEC region. The effect of anisotropy of the inter-site e-p interaction is shown in Fig. 7(a), where α_x is fixed at 1.1 and α_y is varied. Increasing either α_x or α_y separately strengthens the PEC, as shown in Fig. 7(a), where the α_y/α_x ratio is varied. The AFM–PEC phase diagram is relatively insensitive to the ratio of t_y/t_x. In Fig. 7(b), t_x is fixed at 1 and the value of t_y is varied—the resulting t'_c does not depend sensitively on the choice of t_y/t_x.

Summarizing sections III(a)-(d), we see the PEC state in our calculations for a wide range of parameters. In every case, we first arrived at parameters that placed the system in the AFM or WC phases in the $t' = 0$ limit, and then varied only t'. Thus the transition to PEC is a consequence of frustration alone. With variation of e-p coupling and Coulomb interactions, the amount of frustration needed to drive the AFM–PEC transition can vary over a sizable range of frustration. We will discuss the implications of this further in relationship to the CTS materials further in section IV.

E. Finite-size issues

We have performed several checks on our calculations that indicate that the PEC state found in our numerical calculations is an intrinsic property of Eq. 1 and *not* induced by finite size effects.

(i) Noninteracting bandstructure: One common finite-size effect in numerical calculations are changes in the Fermi-level degeneracy or level crossings of the noninteracting system. In the lattice of Fig. 2(a) the Fermi level degeneracy does not change throughout the range $0 < t' < 1$, remaining 2-fold degenerate throughout this range. This degeneracy is broken by x-axis dimerization, shown in Fig. 2(b), giving a nondegenerate Fermi level for $0 < t' < 1$. At $t' = 1$ the degeneracy at the Fermi level increases to 6-fold; in the presence of interactions the ground state can become triplet (S=1) for $t' \gtrsim 0.8$. Hence we stop at $t' \lesssim 0.8$ where the ground state is $S = 0$.

(ii) Interactions: As mentioned above, no transition occurs for $U = V_{ij} = 0$. This further indicates that the transition is not a feature of the single-particle bandstructure.

(iii) Commensurability: We have verified that the PEC state does not occur for electron densities different from $\rho = \frac{1}{2}$; for example, no transition to PEC or any "nonmetallic" state occurs for 6 or 10 electrons on the 4×4 lattice.

IV. APPLICATION TO REAL MATERIALS

In the following we discuss how our theory applies to real materials, and may even give insight to the mechanism of correlated-electron superconductivity in $\rho = \frac{1}{2}$ materials.

A. Application to organic CTS

The superconducting organic CTS share many characteristics of other strongly-correlated superconductors, in particular the high-T_c cuprates, including reduced dimensionality and the presence of AFM near SC. At the same time, SC in the CTS occurs under pressure at a constant carrier density of $\rho = \frac{1}{2}$ rather than under the influence of doping. A variety of exotic insulating states *in addition to AFM*, including CO[66] and spin-gapped states[67,68], as well as possible QSL states[69], are proximate to the superconducting state in the CTS. Our work shows that only the AFM phase is described by the dimer Mott-Hubbard model. Since in all cases the experimental systems are structurally related, with identical or near-identical molecular components, we believe that the same mechanism of SC should apply to them. In Reference 8 we had pointed out how the PEC concept can perhaps lead to such a unifying theory. Here we expand on this theme.

1. CTS with PEC insulating states

We briefly review here experimental evidence for PEC formation in several 2D CTS families.

(i) θ-(ET)$_2$X: CO corresponding to the PEC and spin gap are found in the θ-$(ET)_2MM'(SCN)_4$ family[67]. In MM'=RbZn, the CO occurs below the MI transition at $T \sim$190K, while the SG appears below 20K[67]. The charge order pattern in the CO phase below the MI transition has been experimentally determined for MM'=RbZn and follows a horizontal stripe pattern (see Fig. 6 in Reference 70). The horizontal CO is definitely not the WC. Rather, the CO pattern is precisely as expected in the PEC, with $\cdots 1100 \cdots$ CO along the two directions of largest hopping (the p-directions in the θ-$(ET)_2X$ lattice), and $\cdots 1010 \cdots$ order along the direction of weakest hopping (c-direction in θ-$(ET)_2X$). Experiments have revealed that with decreasing temperature, the c-axis lattice parameter decreases[71]. The decrease in the lattice parameter implies increased carrier hopping in this direction and therefore increased frustration within our theory, giving the transition to the singlet PEC and observed spin gap.

(ii) α-(ET)$_2$X: The crystal structure of α-$(ET)_2X$ is quite similar to that of θ-$(ET)_2X$. The existence of a SG opening below 136K has been known for some time in α-$(ET)_2I_3$[72]. Below the 136K transition CO is found which has been confirmed to be of the same pattern as in θ-$(ET)_2X$; see for example Fig. 2 in Reference 73.

(iii) β-(meso-DMET)$_2PF_6$: This 2D CTS exhibits a pressure-induced transition from CO to SC[74,75]. While the charge order pattern in this CTS is referred to as "checkerboard" by the authors, the checkerboard pattern refers to meso-DMET *dimers* as units. In terms of meso-DMET *monomer* units, the CO pattern is the same as the PEC in Fig. 2(c), with $\cdots 1100 \cdots$ in two directions and $\cdots 1010 \cdots$ along the third direction (see Fig. 2 in Reference 75.)

(iv) β'-X[Pd(dmit)$_2$]$_2$: In this family the materials dmit molecules are arranged in dimers. The frustration varies with the cation X, with the least frustrated in the series showing AFM order[76]. Among the materials with larger frustration, $X = EtMe_3P$ has a SG transition at 25K to what has been described as a VBS state[77]. The experimentally

determined bond and charge distortion patterns (see Fig. 3(b) in Reference 77) are exactly as expected for the PEC, with period 4 charge and bond distortions along what is the x axis in Fig. 2. The intradimer charge disproportionation in particular argues against the SG state from being a simple VBS, which would require equal charge densities on all the molecules.

2. *κ-$(ET)_2Cu_2(CN)_3$ and $EtMe_3Sb[Pd(dmit)_2]_2$: QSL or charge-disproportionated states?*

There has been much recent interest in these CTS[69] specifically because they present possible realizations of the long awaited QSL[48–56]. In both cases the materials have nearly isotropic triangular lattices of dimer unit cells (corresponding to Fig. 2(b) with $t' = 1$) within an effective $\rho = 1$ model. In κ-$(ET)_2Cu_2(CN)_3$ (hereafter κ-CN) the estimate for the Heisenberg exchange integral between n.n. dimers is $J \sim$220–250 K[78,79]. ^{1}H NMR experiments find absence of long range magnetic order down to 32 mK[78]. Very similar behavior is also seen in $EtMe_3Sb[Pd(dmit)_2]_2$ (hereafter dmit-Sb)[80]. The insulating ground state in κ-CN is close to SC, transition to superconductivity occurring under moderate pressure[81]. SC is found in the dmit family as well[82].

Recent experiments in both κ-CN and dmit-Sb have found peculiarities that appear to be unexpected within QSL theories. Below we list experiments that seem to indicate that apparent QSL behavior at low temperatures is giving way to a "hidden order", and perhaps even charge disproportionation, which by itself would be against spin-only models.

(i) A second order phase transition is seen at 6 K in κ-CN in measurements of heat-capacity C_p[83], ^{13}C NMR relaxation rate $1/T_1$[84], and lattice expansion coefficients[85]. The last experiment finds strong lattice effects at the transition, indicating possible role of charge degrees of freedom[85]. A symmetry-breaking and/or topological ordering transition at T < 1 K has also been observed in dmit-Sb[80].

(ii) The specific heat C_p in κ-CN is linear in T for T between 0.75 and 2.5 K, indicating a gapless energy spectrum[83]. The Sommerfeld coefficient γ is nonzero and large even at T =75 mK[83]. Equally perplexingly, C_p is independent of magnetic field up to 8 T, indicating absence of Zeeman coupling of spins to the field[83]. In contrast, thermal conductivity measurements down to 80 mK indicate a spin gap[86].

(iii) The temperature dependence of the thermal conductivity of dmit-Sb suggests gapless mobile excitations, but magnetic field dependence of the thermal conductivity again indicates a gap[87]. Taken together, (ii) and (iii) suggest gapless spin-singlet excitations but gapped spin-triplet excitations in κ-CN and perhaps also dmit-Sb.

(iv) Measurements of dielectric response in κ-CN have shown increasing and frequency-dependent dielectric constant below 60 K, and possible antiferroelectric ordering of dipoles at $T_c \sim$6 K[88]. Similar dielectric response has also been observed in dmit-Sb[89]. Ferro or antiferroelectric ordering require unequal site charges on the molecules within the dimer unit cells[88,90]. It may be relevant in this context that ^{13}C-NMR experiments on both κ-CN[84] and dmit-Sb[91] find unusual line broadenings at low T that cannot be ascribed to disorder[92], which might also indicate charge disproportionation. Similar line broadening at low T in $EtMe_3P[(dmit)_2]_2$ occurs at the transition to the PEC[77], which in turn gives way to superconductivity under pressure[82].

Whether or not there exists a fundamental difference between κ-CN and dmit-Sb, or whether the difference lies in only having a smaller gap in dmit-Sb in which T_c is 1K as opposed to 6K, is currently not entirely obvious. Lattice expansion studies in dmit-Sb (or other measurements of electron-lattice interaction), and perhaps also additional low temperature NMR measurements are needed here. Interestingly, a recently published phase diagram of β'-$Pd(dmit)_2$ salts places dmit-Sb at the interface of AFM and strongly CO phases[69]. The close proximity to CO suggests tendency to charge disproportionation even in dmit-Sb. Note that any difference between κ-CN and dmit-Sb supports the $\rho = \frac{1}{2}$ model, since the simple description as a triangular lattice of dimers is no longer enough and the detailed couplings between the monomers in the materials are indeed different because of their different crystal structures.

Although it is as yet not entirely clear whether or not existing spin-liquid models[48–56] with appropriate modifications can explain the above anomalies, it appears that for κ-CN and possibly dmit-Sb, spin degrees of freedom alone cannot describe the low temperature (below 6K in κ-CN and below 1K in dmit-Sb) properties. Rather, any description of the ground state must involve charge as well as spin degrees of freedom. Assuming that the above experiments and their interpretations are correct, the proper theoretical model should have built-in significant electron-lattice coupling and should lead to charge disproportionation and excitation energy spectrum with gapless singlet excitations and gapped spin excitations. We believe that the highly frustrated $\rho = \frac{1}{2}$ model satisfies all of the above criteria, in addition to providing the starting point for a theory of superconductivity in the CTS (see below). T-linear specific heat but gapped magnetic susceptibility were noted in nonmetallic vanadium bronzes[93] as far back as 1978, and at the time was considered to be a distinctive proof for bipolarons. The nonzero spin-singlet degeneracy within this model comes from tunneling motion of the bipolarons, causing them to "flip flop" between equivalent configurations[93]. We propose that a similar mechanism is at play in the present case at large t'. Particularly in κ-CN the lattice structure and

the orientations of molecules are such that the spin-singlet bonds, which occur between monomers belonging to two neighboring dimers can flip flop between the monomers (see Fig. 4 in Reference 8.) Within our proposed picture for κ-CN, the transition at 6K is to the spin-singlet charge-disproportionated state, with short range fluctuating order. Magnetic excitations even in this state, however, require breaking the spin-singlet bonds.

Several recent theoretical works[94–96] have also considered intradimer charge degrees of freedom in κ-CN, in view of the possible phase transition at 6 K, and in particular, the dielectric anomaly reported in reference 88. References 94 and 95 investigated the strong-dimer limit of the $\rho = \frac{1}{2}$ extended Hubbard model, where the Hilbert space in lowest order is restricted to states with one hole per dimer, and interactions between dimers are treated as perturbations. Different CO patterns, and charge or spin liquid states with short-range order, depending on the relative magnitudes of the interdimer Coulomb interactions and the intradimer hopping were found by Hotta. κ-CN below 6 K within this model is a short-range ordered state with fluctuating dipoles and spins. Naka and Ishihara considered a similar model in the mean-field and classical limits; as a function of temperature several possible combinations of CO and spin ordering were found[95]. Gomi *et al's.* work is closest to ours. The author's consider the $\rho = \frac{1}{2}$ extended Hubbard model specifically for the κ-lattice (thus the strongly frustrated region of our model), and find from exact diagonalization that for nonzero electron-lattice coupling the ground state was a CO ferroelectric near the AFM-PM phase boundary[96]. The possibility of unequal charge distributions within the dimers[94–96] is in agreement with our results. The key differences from our work with these theories are that frustration as well as strength of the intradimer bonds are variables within our model, and our determination that the formation of the CO is driven by the tendency to the form spin-singlets. Finally, we suggest that this singlet formation is related to transition to superconductivity (see below).

3. Consequence of stronger frustration—paired electron liquid and superconductivity

As mentioned above, numerical results for $t' \gtrsim 0.8$ are not useful due to the highly degenerate ground state becoming spin-triplet in our finite clusters. We have suggested elsewhere that the occupied spin-singlet bonded '1–1' sites of the PEC can be thought of as *effective* single sites doubly occupied by charge carriers, and similarly the pairs of '0–0' vacancies can be thought of as single vacant sites[97]. Such a mapping would transform the PEC to an effective checkerboard CO with alternate sites (in the square lattice representation) occupied by double occupancies and vacancies. The effective Hamiltonian that describes the checkerboard CO in this case is a $\rho = 1$ extended Hubbard model with weak *attractive* U whose origin is the exchange interaction that stabilizes the singlet bond within the original $\rho = \frac{1}{2}$ Hamiltonian. The n.n. interaction within the effective Hamiltonian remains repulsive to simulate the checkerboard ordering of the effective doubly occupied sites.

While such a mapping is not rigorous, similar mapping of n.n. spin-bonded sites to double occupancies has been routinely used in the literature on bipolaron models[98,99]. The difference between our work and traditional bipolaron models is that the spin-singlet bonding within our work is driven primarily by AFM correlations, while within the bipolaron models it is a consequence of effective attraction due to the overscreening of the e-e repulsion by e-p interactions[99,100]. We have investigated the consequences of stronger frustration[101] in the $\rho = \frac{1}{2}$ anisotropic triangular lattice within the effective $\rho = 1$ extended Hubbard model with attractive U[97]. We found a CO-to-SC transition within the effective model[97], suggesting a PEC-to-SC transition within the $\rho = \frac{1}{2}$ model with repulsive interactions. Although this result is not a proof of transition to SC within the repulsive $\rho = \frac{1}{2}$ model, it nevertheless is instructive and provides the direction for future research.

Demonstration of SC within the actual model will require further work. What is interesting though is that the proposed scenario can give a unified approach to SC in all organic CTS, irrespective of whether the insulating state proximate to SC is AFM[102], CO[67,103] or VBS[82]. Recall that within existing mean field theories the AFM-to-SC transition is driven by spin fluctuations[13–23], while the CO-to-SC transition is driven by charge fluctuations[65]. Even if we ignore that recent precise numerical calculations[25–27] have demonstrated the absence of SC within the proposed spin-fluctuation models in this context (thereby raising doubts also about mean-field theory of charge-fluctuation mediated superconductivity), different mechanisms of SC for structurally related materials with identical or near-identical molecular components appear to be unrealistic. Within our proposed scenario, the charge-ordered or VBS systems that exhibit SC are PECs in the semiconducting state, while the AFM systems under pressure transform to PECs first and then to SC (although due to actual crystal structures the "width" of the PEC region could be narrow to vanishing within the latter). The SC phase within this scenario is a paired-electron liquid. There is considerable overlap between these ideas and the one proposed by Moulopoulos and Ashcroft for the continuous electron gas[46,47].

B. Application to inorganic $\rho = \frac{1}{2}$ materials

The thrust of our work has been to understand within a unified theoretical approach the variety of exotic insulating states that are proximate to the superconducting state in 2:1 cationic or 1:2 anionic 2D CTS. We have shown here that the peculiarities of these materials originate from the unique behavior of $\rho = \frac{1}{2}$ in the presence of both strong e-e interactions and lattice frustration. It is conceivable that the complex behavior of apparently unrelated inorganic families can be understood within the same broad theoretical approach. We list two such classes of materials below to point out the hitherto unnoticed similarities between them and $\rho = \frac{1}{2}$ CTS.

1. Layered cobaltates

Layered cobaltates Na_xCoO_2 have attracted wide attention because of their 2D structure, tunable carrier concentration, and the occurrence of SC[40]. The Co ions form a 2D triangular lattice, are in their low-spin state, and their valence ranges from Co^{3+} at $x = 1$ to Co^{4+} at $x = 0$. Charge carriers are $S = \frac{1}{2}$ holes on the Co^{4+} sites and the hole density $\rho = 1 - x$. Trigonal distortion splits the occupied t_{2g} orbitals into e'_g and a_{1g} orbitals. LDA calculations have suggested that although for large x the e'_g orbitals occur below the Fermi level and an a_{1g}-only description is valid, this description breaks down at small x where e'_g orbitals can be nearly degenerate[104,105]. In contrast, correlated-electron calculations find that the a_{1g} – e'_g energy separation is positive and relatively large for all x[106,107], suggesting that low energy excitations can likely be described within a_{1g}-only single-band models.

The temperature dependent magnetic susceptibility $\chi(T)$ shows a peculiar ρ-dependence within the family, with small ρ (large x) exhibiting strongly correlated behavior and large ρ (small x) exhibiting weakly correlated behavior[108]. We have recently shown that ρ-dependent $\chi(T)$, exactly as seen in the cobaltates, is expected within the single-band extended Hubbard model on a triangular lattice[109]. Equally interestingly, $\chi(T)$ behavior in Na_xCoO_2 is very similar to that in the family of CTS as a whole, where also $\chi(T)$ shows a systematic ρ-dependence that is understood within the single-band extended Hubbard model[110]. It is tempting to compare now the superconducting states in hydrated cobaltates and CTS with this apparent similarity in mind.

Although superconductivity in $Na_xCoO_2 \cdot yH_2O$ occurs at $x \simeq 0.35$[40], it is now established that the Co-ion valency here is determined not only by the Na content, but also by H_3O^+ ions. There have been several reports that SC here occurs over a very narrow range of hole density ρ, and that maximum T_c occurs at or very close to Co-ion valency 3.5+, corresponding to $\rho = \frac{1}{2}$[111–113]. If this is confirmed from future experimental work, it would appear that like the CTS, cobaltates are yet another example of a frustrated 2D $\rho = \frac{1}{2}$ superconductor, suggesting that the mechanism of SC in the two families is related.

2. $\rho = \frac{1}{2}$ spinels

The B sublattice in spinel compounds AB_2X_4 form a frustrated three-dimensional (3D) pyrochlore lattice and usually consist of transition metal cations that possess partially filled t_{2g} d-orbitals. For integer occupancies of d-electrons per B cation the geometrical degeneracy of the underlying lattice is often lifted by orbital ordering (OO), leading to formation of spin-singlet dimers. Only four of the many spinel compounds are superconducting, of which three have effective carrier density $\rho = \frac{1}{2}$: $LiTi_2O_4$, $CuRh_2S_4$, and $CuRh_2Se_4$. In $LiTi_2O_4$ there is one d-electron per two $Ti^{3.5+}$ ions; in $CuRh_2S_4$ and $CuRh_2Se_4$ the $Rh^{3.5+}$ ions have average d-hole occupancy of $\frac{1}{2}$. Jahn-Teller instability or OO can lead to occupancy of the same t_{2g} orbitals, making the filled bands exactly $\frac{1}{4}$-filled, as in the superconducting organic CTS (the apparently different spinel superconductor CuV_2S_4, also has noninteger number of d-electrons per $V^{3.5+}$ ion.)

Yet another similarity between the organics and the $\rho = \frac{1}{2}$ spinels is the proximity of the superconducting state to exotic semiconducting states. Thus $CuIr_2S_4$ and $LiRh_2O_4$, both isoelectronic with $CuRh_2S_4$, undergo MI transitions that are accompanied by CO. In $CuIr_2S_4$ the Ir ions are charge-ordered as Ir^{3+}-Ir^{3+}-Ir^{4+}-Ir^{4+} along specific directions[114]. This would correspond exactly to the $\cdots 0011 \cdots$ CO in our notation here. As in the 2D PEC, these inorganic 3D systems are spin-gapped due to the formation of Ir^{4+}-Ir^{4+} singlet bonds. It is interesting to recall that similar singlet bonds between Ti^{3+} ions had been proposed[93,115] many years back within bipolaron theories of Ti_4O_7 and $LiTi_2O_4$. As explicitly shown in our work here, the singlet bond formation is a natural consequence of frustration and $\frac{1}{4}$-filling. Work is currently in progress to extend the PEC concept to the checkerboard lattice, thought to be 2D equivalents of the pyrochlore lattice, multiple orbitals per site[116].

V. CONCLUSIONS

In summary, there is an extraordinarily strong tendency to form spin-singlets in systems with charge carrier concentration precisely $\frac{1}{2}$. Naturally, in $\rho = \frac{1}{2}$ this spin-singlet state is accompanied by CO. The stability of the PEC derives from the commensurability of the PEC at $\rho = \frac{1}{2}$. In the anisotropic triangular lattice, the PEC consists of charge arrangements $\cdots 1100 \cdots$ in two directions and $\cdots 1010 \cdots$ in the third direction. Thus although $\rho = \frac{1}{2}$ in principle is incommensurate on the triangular lattice, "separately commensurate" periodic charge arrangements are nevertheless possible.

VI. ACKNOWLEDGMENTS

We thank M. Abdel-Jawad, H. Fukuyama, K. Kanoda, and R. Kato for helpful discussions. This work was supported by the US Department of Energy grant DE-FG02-06ER46315. RTC thanks the University of Arizona for support while on sabbatical.

[1] E. H. Lieb and F. Y. Wu, Phys. Rev. Lett. **20**, 1445 (1968).
[2] T. Kashima and M. Imada, J. Phys. Soc. Jpn. **70**, 3052 (2001).
[3] H. Morita, S. Watanabe, and M. Imada, J. Phys. Soc. Jpn. **71**, 2109 (2002).
[4] T. Ohashi, N. Kawakami, and H. Tsunetsugu, Phys. Rev. Lett. **97**, 066401 (2006).
[5] J. Hubbard, Phys. Rev. B **17**, 494 (1978).
[6] K. Penc and F. Mila, Phys. Rev. B **49**, 9670 (1994).
[7] H. Seo and H. Fukuyama, J. Phys. Soc. Jpn. **66**, 1249 (1997).
[8] H. Li, R. T. Clay, and S. Mazumdar, J. Phys.: Condens. Matter **22**, 272201 (2010).
[9] R. Moessner and A. P. Ramirez, Physics Today **59**, 24 (2006).
[10] L. Balents, Nature **464**, 199 (2010).
[11] P. W. Anderson, Mater. Res. Bull. **8**, 153 (1973).
[12] P. Fazekas and P. W. Anderson, Phil. Mag. **30**, 423 (1974).
[13] M. Vojta and E. Dagotto, Phys. Rev. B **59**, R713 (1999).
[14] J. Schmalian, Phys. Rev. Lett. **81**, 4232 (1998).
[15] H. Kino and H. Kontani, J. Phys. Soc. Jpn. **67**, 3691 (1998).
[16] H. Kondo and T. Moriya, J. Phys. Soc. Jpn. **67**, 3695 (1998).
[17] B. J. Powell and R. H. McKenzie, Phys. Rev. Lett. **94**, 047004 (2005); ibid **98**, 027005 (2007).
[18] G. Baskaran, Phys. Rev. Lett. **90**, 197007 (2003).
[19] J. Y. Gan, Y. Chen, Z. B. Su, and F. C. Zhang, Phys. Rev. Lett. **94**, 067005 (2005).
[20] J. Y. Gan, Y. Chen, and F. C. Zhang, Phys. Rev. B **74**, 094515 (2006).
[21] P. Sahebsara and D. Sénéchal, Phys. Rev. Lett. **97**, 257004 (2006).
[22] T. Watanabe, H. Yokoyama, Y. Tanaka, and J. Inoue, J. Phys. Soc. Jpn. **75**, 074707 (2006).
[23] B. Kyung and A. M. S. Tremblay, Phys. Rev. Lett. **97**, 046402 (2006).
[24] T. Ishiguro, K. Yamaji, and G. Saito, *Organic Superconductors* (Springer-Verlag, New York, 1998).
[25] T. Mizusaki and M. Imada, Phys. Rev. B **74**, 014421 (2006).
[26] R. T. Clay, H. Li, and S. Mazumdar, Phys. Rev. Lett. **101**, 166403 (2008).
[27] L. F. Tocchio, A. Parola, C. Gros, and F. Becca, Phys. Rev. B **80**, 064419 (2009).
[28] D. A. Huse and V. Elser, Phys. Rev. Lett. **60**, 2531 (1988).
[29] T. Jolicoeur and J. C. Le Guillou, Phys. Rev. B **40**, 2727 (1989).
[30] R. R. P. Singh and D. A. Huse, Phys. Rev. Lett. **68**, 1766 (1992).
[31] C. Zeng and V. Elser, Phys. Rev. B **42**, 8436 (1990).
[32] S. Ryu, O. I. Motrunich, J. Alicea, and M. P. A. Fisher, Phys. Rev. B **75**, 184406 (2007).
[33] Y. Ran, M. Hermele, P. A. Lee, and X.-G. Wen, Phys. Rev. Lett. **98**, 117205 (2007).
[34] M. Hermele, Y. Ran, P. A. Lee, and X.-G. Wen, Phys. Rev. B **77**, 224413 (2008).
[35] M. B. Hastings, Phys. Rev. B **63**, 014413 (2000).
[36] R. Budnik and A. Auerbach, Phys. Rev. Lett. **93**, 187205 (2004).
[37] R.R.P Singh and D.A. Huse, Phys. Rev. B **76**, 180407 (2007); ibid, **77**, 144415 (2008).
[38] G. Evenbly and G. Vidal, Phys. Rev. Lett. **104**, 187203 (2010).
[39] C.K. Majumdar and D.K. Ghosh, Phys. Rev. B **10**, 1388 (1969); ibid **10**, 1399 (1969).
[40] K. Takada, H. Sakurai, E. Takayama-Muromachi, F. Izumi, R. A. Dilanian, and T. Sasaki, Nature **422**, 53 (2003).
[41] O. I. Motrunich and P. A. Lee, Phys. Rev. B **70**, 024514 (pages 8) (2004).
[42] T.-P. Choy, D. Galanakis, and P. Phillips, Phys. Rev. B **75**, 073103 (2007).

[43] J. Merino, B. J. Powell, and R. H. McKenzie, Phys. Rev. B **79**, 161103 (2009).
[44] H. Kino and H. Fukuyama, J. Phys. Soc. Jpn. **64**, 2726 (1995); ibid **65**, 2158 (1996).
[45] R. H. McKenzie, Science **278**, 820 (1997).
[46] K. Moulopoulos and N. W. Ashcroft, Phys. Rev. Lett. **69**, 2555 (1992).
[47] K. Moulopoulos and N. W. Ashcroft, Phys. Rev. B **48**, 11646 (1993).
[48] S.-S. Lee and P. A. Lee, Phys. Rev. Lett. **95**, 036403 (2005).
[49] O. I. Motrunich, Phys. Rev. B **72**, 045105 (2005).
[50] V. Galitski and Y. B. Kim, Phys. Rev. Lett. **99**, 266403 (2007).
[51] S.-S. Lee, P. A. Lee, and T. Senthil, Phys. Rev. Lett. **98**, 067006 (2007).
[52] P. A. Lee, Reports on Progress in Physics **71**, 012501 (2008).
[53] Y. Qi and S. Sachdev, Phys. Rev. B **77**, 165112 (2008).
[54] Y. Qi, C. Xu, and S. Sachdev, Phys. Rev. Lett. **102**, 176401 (2009).
[55] C. Xu and S. Sachdev, Phys. Rev. B **79**, 064405 (2009).
[56] T. Grover, N. Trivedi, T. Senthil, and P. A. Lee, Phys. Rev. B **81**, 245121 (2010).
[57] R. T. Clay, S. Mazumdar, and D. K. Campbell, Phys. Rev. B **67**, 115121 (2003).
[58] R. T. Clay, R. P. Hardikar, and S. Mazumdar, Phys. Rev. B **76**, 205118 (2007).
[59] K. C. Ung, S. Mazumdar, and D. Toussaint, Phys. Rev. Lett. **73**, 2603 (1994).
[60] C. Rovira, Chem. Eur. J. **6**, 1723 (2000).
[61] R. T. Clay and S. Mazumdar, Phys. Rev. Lett. **94**, 207206 (2005).
[62] G. Beni and P. Pincus, J. Chem. Phys. **57**, 3531 (1972).
[63] J. Merino, H. Seo, and M. Ogata, Phys. Rev. B **71**, 125111 (2005).
[64] M. Kuwabara, H. Seo, and M. Ogata, J. Phys. Soc. Jpn. **72**, 225 (2003).
[65] J. Merino and R. H. McKenzie, Phys. Rev. Lett. **87**, 237002 (2001).
[66] T. Takahashi, Y. Nogami, and K. Yakushi, J. Phys. Soc. Jpn. **75**, 051008 (2006).
[67] H. Mori, J. Phys. Soc. Jpn. **75**, 051003 (2006).
[68] M. Tamura and R. Kato, Sci. Technol. Adv. Mater. **10**, 024304 (2009).
[69] K. Kanoda and R. Kato, Annu. Rev. Condens. Matter Phys. **2**, 167 (2011).
[70] M. Watanabe, Y. Noda, Y. Nogami, and H. Mori, J. Phys. Soc. Jpn. **73**, 116 (2004).
[71] M. Watanabe, Y. Noda, Y. Nogami, and H. Mori, J. Phys. Soc. Jpn. **76**, 124602 (2007).
[72] B. Rothaemel, L. Forró, J. R. Cooper, J. S. Schilling, M. Weger, P. Bele, H. Brunner, D. Schweitzer, and H. J. Keller, Phys. Rev. B **34**, 704 (1986).
[73] N. Tajima and K. Kajita, Science and Technology of Advanced Materials **10**, 024308 (2009).
[74] S. Kimura, T. Maejima, H. Suzuki, R. Chiba, H. Mori, T. Kawamoto, T. Mori, H. Moriyama, Y. Nishio, and K. Kajita, Chem. Commun. **2004**, 2454 (2004).
[75] S. Kimura, H. Suzuki, T. Maejima, H. Mori, J. Yamaura, T. Kakiuchi, H. Sawa, and H. Moriyama, J. Am. Chem. Soc. **128**, 1456 (2006).
[76] R. Kato, Chem. Rev. **104**, 5319 (2004).
[77] M. Tamura, A. Nakao, and R. Kato, J. Phys. Soc. Jpn. **75**, 093701 (2006).
[78] Y. Shimizu, K. Miyagawa, K. Kanoda, M. Maesato, and G. Saito, Phys. Rev. Lett. **91**, 107001 (2003).
[79] W. Zheng, R. R. P. Singh, R. H. McKenzie, and R. Coldea, Phys. Rev. B **71**, 134422 (2005).
[80] T. Itou, A. Oyamada, S. Maegawa, and R. Kato, Nature Phys. **6**, 673 (2010).
[81] T. Komatsu, N. Matsukawa, T. Inoue, and G. Saito, J. Phys. Soc. Jpn. **65**, 1340 (1996).
[82] Y. Shimizu, H. Akimoto, H. Tsujii, A. Tajima, and R. Kato, Phys. Rev. Lett. **99**, 256403 (2007).
[83] S. Yamashita, Y. Nakazawa, M. Oguni, Y. Oshima, H. Nojiri, Y. Shimizu, K. Miyagawa, and K. Kanoda., Nature Phys. **4**, 459 (2008).
[84] Y. Shimizu, K. Miyagawa, K. Kanoda, M. Maesato, and G. Saito, Phys. Rev. B **73**, 140407(R) (2006).
[85] R. S. Manna, M. de Souza, A. Brühl, J. A. Schlueter, and M. Lang, Phys. Rev. Lett. **104**, 016403 (2010).
[86] M. Yamashita, N. Nakata, Y. Kasahara, T. Sasaki, N. Yoneyama, N. Kobayashi, S. Fujimoto, T. Shibauchi, and Y. Matsuda, Nature Phys. **5**, 44 (2009).
[87] M. Yamashita, N. Nakata, Y. Senshu, M. Nagata, H. M. Yamamoto, R. Kato, T. Shibauchi, and Y. Matsuda, Science **328**, 1246 (2010).
[88] M. Abdel-Jawad, I. Terasaki, T. Sasaki, N. Yoneyama, N. Kobayashi, Y. Uesu, and C. Hotta, Phys. Rev. B **82**, 125119 (2010).
[89] M. Abdel-Jawad, (private communication).
[90] H. Seo, J. Phys. Soc. Jpn., JPSJ Online—News and Comments, June 10, 2010.
[91] T. Itou, A. Oyamada, S. Maegawa, M. Tamura, and R. Kato, Phys. Rev. B **77**, 104413 (2008).
[92] K. Gregor and O. I. Motrunich, Phys. Rev. B **77**, 184423 (2008).
[93] B. K. Chakraverty, M. J. Sienko, and J. Bonnerot, Phys. Rev. B **17**, 3781 (1978).
[94] C. Hotta, Phys. Rev. B **82**, 241104 (2010).
[95] M. Naka and S. Ishihara, J. Phys. Soc. Jpn. **79**, 063707 (2010).
[96] H. Gomi, T. Imai, A. Takahashi, and M. Aihara, Phys. Rev. B **82**, 035101 (2010).
[97] S. Mazumdar and R. T. Clay, Phys. Rev. B **77**, 180515(R) (2008).
[98] A. Alexandrov and J. Ranninger, Phys. Rev. B **23**, 1796 (1981).
[99] R. Micnas, J. Ranninger, and S. Robaszkiewicz, Rev. Mod. Phys. **62**, 113 (1990).

[100] A. S. Alexandrov and N. F. Mott, *High Temperature Superconductors And Other Superfluids* (Taylor and Francis, London, 1994).
[101] Note that the ratio t'/t commonly used to measure the degree of frustration in an effective $\rho = 1$ model is not the same as the t'/t considered here for the $\rho = \frac{1}{2}$ lattice.
[102] K. Kanoda, J. Phys. Soc. Jpn. **75**, 051007 (2006).
[103] N. Tajima et al., J. Phys. Soc. Jpn. **75**, 051010 (2006).
[104] D. J. Singh, Phys. Rev. B **61**, 13397 (2000).
[105] K.-W. Lee and W. E. Pickett, Phys. Rev. B **72**, 115110 (2005).
[106] A. Bourgeois, A. A. Aligia, and M. J. Rozenberg, Phys. Rev. Lett. **102**, 066402 (2009).
[107] S. Landron and M. B. Lepetit, Phys. Rev. B **77**, 125106 (2008).
[108] M. L. Foo, Y. Wang, S. Watauchi, H. W. Zandbergen, T. He, R. J. Cava, and N. P. Ong, Phys. Rev. Lett. **92**, 247001 (2004).
[109] H. Li, R. T. Clay, and S. Mazumdar (2010), preprint http://arxiv.org/abs/1012.3118.
[110] S. Mazumdar and A. N. Bloch, Phys. Rev. Lett. **50**, 207 (1983).
[111] P. W. Barnes et al., Phys. Rev. B **72**, 134515 (2005).
[112] H. Sakurai et al., Phys. Rev. B **74**, 092502 (2006).
[113] M. Bañobre-López et al., J. Am. Chem. Soc. **131**, 9632 (2009).
[114] P. G. Radaelli, Y. Horibe, M. J. Gutmann, H. Ishibashi, C. H. Chen, R. M. Ibberson, Y. Koyama, Y.-S. Hor, V. Kiryukhin, and S.-W. Cheong, Nature **416**, 155 (2002).
[115] S. Lakkis, C. Schlenker, B. K. Chakraverty, R. Buder, and M. Marezio, Phys. Rev. B **14**, 1429 (1976).
[116] R. T. Clay, H. Li, S. Sarkar, S. Mazumdar, and T. Saha-Dasgupta, Phys. Rev. B **82**, 035108 (2010).